DOI: 10.37943/15DLPO1951

Assiya Sarinova
PhD, Associate Professor, Department of Intelligent Systems and Cybersecurity
a.sarinova@astanait.edu.kz, orcid.org/0000-0003-4254-376X
Astana IT University, Kazakhstan

Alexandr Neftissov
PhD, Associate Professor, Research and Innovation Center "Industry 4.0"
Alexandr.neftissov@astanait.edu.kz, orcid.org/0000-0003-4079-2025
Astana IT University, Kazakhstan

Leyla Rzayeva
PhD, Associate Professor, Department of Intelligent Systems and Cybersecurity
l.rzayeva@astanait.edu.kz, orcid.org/0000-0003-4254-376X
Astana IT University, Kazakhstan

Lalita Kirichenko
PhD candidate, junior researcher, Research and Innovation Center "Industry 4.0"
lalita17021996@gmail.com, orcid.org/0000-0001-7069-5395
Astana IT University, Kazakhstan

Sanzhar Kusdavletov
MSc, Senior Lecturer, Department of Intelligent Systems and Cybersecurity
sanzhar.kusdavletov@astanait.edu.kz, orcid.org/0000-0003-0286-776X
Astana IT University, Kazakhstan

Ilyas Kazambayev
PhD candidate, Junior Researcher, Research and Innovation Center "Industry 4.0"
ilyaskazambayevgmail.com, orcid.org/0000-0003-0850-7490
Astana IT University, Kazakhstan

MATHEMATICAL FRAMEWORK FORMULATION AND IMPLEMENTATION FOR HYPERSPECTRAL AEROSPACE IMAGES PROCESSING

Abstract: This paper proposes a preprocessing algorithm for aerospace hyperspectral images based on a mathematical apparatus effectively applied in pre-compression transformation problems. In particular, several methods have been analyzed for hyperspectral image (signal) preprocessing from the point of view of digital signal processing algorithms. These mathematical methods are used for problems of filtering signals from noise of different natures and for compression and restoration of signals after their transmission through communication channels. The results of comparative analysis of preparatory processing of lossy compression algorithms based on wavelet analysis, discrete and orthogonal transforms are also given, demonstrating minimization of loss level of reconstructed decoded images. The performance of the proposed preprocessing algorithms with quality metrics is presented to evaluate the quality of the reconstructed hyperspectral aerospace images. The results of this study can be applied and used in the tasks of special processing of hyperspectral images, as well as fundamental knowledge of mathematical apparatuses of the proposed orthogonal preprocessing, considering the specificity of the data which is very important in obtaining images ready for compression for the subsequent identification of objects of the Earth's surface and using such

Received: 14.08.2023 Accepted: 23.09.2023 Published: 30.09.2023

Scientific Journal of Astana IT University
ISSN (P): 2707-9031 ISSN (E): 2707-904X
VOLUME 15, SEPTEMBER 2023

mathematical transformations at the hyperspectral image preprocessing stage before compression provides efficient archiving of the obtained data, while reducing the communication channel load. Through the use of quality metrics of the reconstructed images, the preprocessing algorithm provides an understanding of the threshold of the peak signal-to-noise ratio value and the efficiency of its application to calculate and minimize the loss rate.

Keywords: hyperspectral images; pre-processing; compression algorithm; mathematical apparatus; discrete conversions; Haar wavelets; Daubechies wavelet; Walsh-Hadamard transformation; quality metric; machine learning; artificial intelligence.

Introduction

Currently, research is actively conducted in hyperspectral aerospace imagery (HAI) processing to solve the tasks of monitoring and identifying various objects of the Earth's surface. At the stage of preliminary image processing, the following tasks are solved: contrast enhancement, resizing, orthorectification, radiometric correction, morphological processing, background removal, noise removal, image quality enhancement, application of filters, segmentation, etc. As the name of the stage "preliminary" processing speaks for itself, it includes methods of primary analysis and processing of Earth remote sensing (ERS) data. Accordingly, at the next stage the solution of specific tasks on recognizing objects belonging to a given class is achieved. Also, it should not be forgotten that the received images from space devices reach hundreds of gigabytes, filling communication channels and network bandwidth is reduced. For such purposes algorithms and methods of compression without loss and with loss of quality when restoring the original images are developed. Therefore, before the compression of HAI itself it is necessary to apply pre-processing, which will increase the coefficients of the compression degree and the quality of the restored images for the solution of the subsequent identification of objects of the earth's surface.

In the aspect of HAI processing, there are existing approaches and certainly achieved results in different applied methods to improve image quality, conversion speed, and data specificity. Thus, in [1, 2], the authors propose a joint spatial-spectral scheme for joint compressed sensing. This scheme collects compressed hyperspectral image data using spatial-spectral hybrid compressed sampling, but there are certain limitations in selecting image quality parameters. Close attention has been paid by researchers in [3, 4] to the development of learning-based hyperspectral image compression methods, which have recently attracted much attention in the field of remote sensing. Such methods require the use of a large number of hyperspectral images during training to optimize all parameters and achieve high compression performance [5, 6].

There are some developments in the field of research of actual problems of preprocessing before compression of aerospace images, which use mathematical apparatuses, for example, Tusker decomposition [7, 8], consideration of spatial and spectral characteristics by PCA methods [9], algorithms of block transformation before compression [10], clustering and regression transformation in lossless compression [11].

At the same time, discrete mathematical transformations are actively used, which are implemented by the authors: in [12] PCA algorithms based on wavelet transformations + the standard JPEG2000 encoder, in [13] an entropy coding algorithm using clustering is presented, researchers in [14] a 3D block coding algorithm based on the SPIHT + wavelet transform algorithm is proposed. The proposed algorithms have positive results in terms of quality metrics, but at the same time there are unsolved problems in the speed of transformations, degrees of compression, as well as the use of incomplete datasets, the authors used only some fragments of aerospace images, which limits the effectiveness of the results of these studies.

DOI: 10.37943/15DLPO1951

Based on the analysis of research sources in the perspective of improving the efficiency of the use of preprocessing based on mathematical transformations, it should be noted the relevance of the study and the existing unresolved problems before compression to solve the problems of identification and subsequent recognition of various objects of the Earth's surface.

The hypothesis of the study is the development of algorithms for the preliminary processing of hyperspectral images in the application of different mathematical apparatuses in a comparative experiment of different hyperspectral aerospace images received through the communication channel to solve the following problems – effective compression after mathematical orthogonal transformations on the degree of compression, compression speed and quality of reconstructed images, as well as in this case in further research to use existing and modify neural network methods for identification and detection Neural networks and machine learning methods are now widely used to solve the problems of identification and recognition, which allow training hyperspectral image data both in the pre-processing and in the compression process.

Pre-processing algorithm for aerospace images.

We analyze on the basis of wavelet and discrete cosine transforms the preprocessing algorithm for subsequent compression, recognition and identification of HAI with minimization of the loss level.

Preparatory processing for lossy HAI compression. Let us consider the preparatory processing based on wavelet and orthogonal transforms before lossless compression of hyperspectral AIs.

Proposed steps for preparatory processing of HAI:

1. Transforming a data structure based on the original HAI storing wavelet coefficient values, using the Haar wavelet as an example [15].

2. Transform a data structure based on the original HAI storing wavelet coefficient values, applying all low-frequency and high-frequency coefficients using the Daubechies wavelet as an example.

3. Transforming a data structure based on the original HAI storing coefficient values, using the discrete cosine transform as an example [16-18].

4. Transforming a data structure based on the original HAI storing coefficient values, using the three-level Walsh-Adamar transform as an example [19-20].

5. Transform the obtained data structures based on steps 1-4 by quantizing wavelet coefficients.

6. Utilizing standard metrics to evaluate quality criteria for restored images PSNR, MSE, MSE, etc.

Transformation based on the coefficients of the Daubechies wavelet

Let us now consider the application of Daubechies wavelet transform in hyper spectral aerospace images (AI) [43, 50]. Wavelet coding methods for Daubechies images employ Haar wavelets in conjunction with concepts such weighted averages and weighted differences.

Let us introduce some notation for the formation of Daubechies wavelet coefficients:

- Daubechies wavelet coefficients $c_0, c_1, c_2, \ldots c_{N-1}$;
- operator L_n – low pass filter;
- operator H_n – high pass filter;
- a matrix of low-frequency and high-frequency wavelet coefficients $(L_n x)_i\ (H_n x)_i$;
- the Daubechies wavelet coefficients are: $C1 = \frac{1+\sqrt{3}}{4\sqrt{2}}\ C2 = \frac{3+\sqrt{3}}{4\sqrt{2}}\ C3 = \frac{3-\sqrt{3}}{4\sqrt{2}}\ C4 = \frac{1-\sqrt{3}}{4\sqrt{2}}$.

Scientific Journal of Astana IT University
ISSN (P): 2707-9031 ISSN (E): 2707-904X
VOLUME 15, SEPTEMBER 2023

Let's explore the specific steps involved in the process of converting hyperspectral AI channel values $\mathrm{I}[m,n,k]$ using the Daubechies wavelet.

Step 1. Calculate low-frequency coefficients based on the original AI of four adjacent values.

$$c_0 \times I[m-1,n-1,k-1]+c_1 \times I[m-2,n-2,k-2]+c_2 \times I[m-3,n-3,k-3]+\ldots+ c_{N-1} \times I[m-N,n-N,k-N] \quad (1)$$

for some set of coefficients $c_0, c_1, \ldots, c_{N-1}, \ N \geq 2$.

Step 2. Similarly, we calculate the operations of subtracting high frequency coefficients

$$c_1 \times I[m-1,n-1,k-1]-c_0 \times I[m-2,n-2,k-2]+c_3 \times I[m-3,n-3,k-3]-c_2 \times I[m-4,n-4,k-4]+\ldots$$

Step 3. Based on step 1, the operator $L_n : R^n \to R^{n/2}$ is defined as follows:

$$(L_n I[m,n,k])_i = \sum_{j=1}^{n} c_{j-2i+1} I[m,n,k]_j, \qquad i=1,\ldots,\frac{n}{2}. \quad (2)$$

Let us now derive the expression for multiplying the coefficient matrix by the values of the original image as:

$$\begin{gathered}
(L_n I[m,n,k])_i = c_{2-2i} \times I[m,n,k]_1 + c_{3-2i} \times I[m,n,k]_2 + \\
c_{4-2i} \times I[m,n,k]_3 + \ldots + c_{n+1-2i} \times I[m,n,k]_n \\
\text{when } i=1, \quad (L_n I[m,n,k])_1 = c_0 \times I[m,n,k]_1 + c_1 \times I[m,n,k]_2 + \\
c_2 \times I[m,n,k]_3 + \ldots + c_{n-1} \times I[m,n,k]_n \\
\text{when } i=2, \quad (L_n I[m,n,k])_2 = c_{-2} \times I[m,n,k]_1 + c_{-1} \times I[m,n,k]_2 + \\
c_0 \times I[m,n,k]_3 + \ldots + c_{n-3} \times I[m,n,k]_n \\
\text{when } i=3, \quad (L_n I[m,n,k])_3 = c_{-4} \times I[m,n,k]_1 + c_{-3} \times I[m,n,k]_2 + \\
c_{-2} \times I[m,n,k]_3 + \ldots + c_{n-5} \times I[m,n,k]_n \\
\ldots\ldots\ldots\ldots\ldots\ldots\ldots\ldots\ldots\ldots\ldots\ldots\ldots\ldots\ldots\ldots\ldots\ldots\ldots\ldots\ldots\ldots\ldots\ldots \\
\text{when } i=\frac{n}{2}, \quad (L_n I[m,n,k])_{\frac{n}{2}} = c_{2-n} \times I[m,n,k]_1 + c_{3-n} \times I[m,n,k]_2 + \\
c_{4-n} \times I[m,n,k]_3 + \ldots + c_1 \times I[m,n,k]_n
\end{gathered} \quad (3)$$

Let us formulate the following matrix of values with low-frequency coefficients:

$$L_n = \begin{pmatrix} c_0 & c_1 & c_2 & c_3 & \ldots & c_{n-1} \\ c_{-2} & c_{-1} & c_0 & c_1 & \ldots & c_{n-3} \\ c_{-4} & c_{-3} & c_{-2} & c_{-1} & \ldots & c_{n-5} \\ c_{2-n} & c_{3-n} & c_{4-n} & c_{5-n} & \ldots & c_1 \end{pmatrix} \quad (4)$$

Step 4. Based on the step 2, the following operator $H_n : R^n \to R^{n/2}$ is defined as follows:

$$(H_n I[m,n,k])_i = \sum_{j=1}^{n} (-1)^{j+1} c_{2i-j} I[m,n,k]_j, \qquad i=1,\ldots,\frac{n}{2}. \quad (5)$$

Let us derive the expression for multiplying the coefficient matrix by the values of the original image:

DOI: 10.37943/15DLPO1951

$$(H_n I[m,n,k])_i = c_{2i-1} \times I[m,n,k]_1 - c_{2i-2} \times I[m,n,k]_2 + c_{2i-3} \times I[m,n,k]_3 - c_{2i-4} \times I[m,n,k]_4 ... + (-1)^{n+1} c_{2i-n} \times I[m,n,k]_n$$

$$\text{when } i=1, \quad (H_n I[m,n,k])_1 = c_1 \times I[m,n,k]_1 - c_0 \times I[m,n,k]_2 + c_{-1} \times I[m,n,k]_3 - c_{-2} \times I[m,n,k]_4 + ... + (-1) c_{2-n} \times I[m,n,k]_n$$

$$\text{when } i=2, \quad (H_n I[m,n,k])_2 = c_3 \times I[m,n,k]_1 - c_2 \times I[m,n,k]_2 + c_1 \times I[m,n,k]_3 - c_0 \times I[m,n,k]_4 + ... + (-1) c_{4-n} \times I[m,n,k]_n \quad (6)$$

$$\text{when } i=3, \quad (H_n I[m,n,k])_3 = c_5 \times I[m,n,k]_1 - c_4 \times I[m,n,k]_2 + c_3 \times I[m,n,k]_3 - c_2 \times I[m,n,k]_4 + ... + (-1) c_{6-n} \times I[m,n,k]_n$$

$$\text{when } i=\frac{n}{2}, \quad (H_n I[m,n,k])_{\frac{n}{2}} = c_{n-1} \times I[m,n,k]_1 - c_{n-2} \times I[m,n,k]_2 + c_{n-3} \times I[m,n,k]_3 - c_{n-4} \times I[m,n,k]_4 + ... + (-1)^{n+1} c_0 \times I[m,n,k]_n .$$

Let us formulate the following matrix of values with low-frequency coefficients:

$$H_n = \begin{pmatrix} c_1 & -c_0 & c_{-1} & -c_{-2} & ... & (-1)^{n+1} \cdot c_{2-n} \\ c_3 & -c_2 & c_{-1} & -c_0 & ... & (-1)^{n+1} \cdot c_{4-n} \\ c_5 & -c_4 & c_{-1} & -c_2 & ... & (-1)^{n+1} \cdot c_{6-n} \\ ..... & & & & & \\ c_{n-1} & -c_{n-2} & c_{n-3} & -c_{n-4} & ... & (-1)^{n+1} \cdot c_0 \end{pmatrix} \quad (7)$$

Step 5. Let us define L_n filter in the form of the matrix for $\mathrm{I}[m,n,k]$. Let us denote by $L_n[i,j]$ an element i, j of the matrix representation of the operator L_n for the sequence of data. Then,

$$L_n[i,j] = \begin{cases} c_{j-2i+1} & \text{when } 0 \le j-2i+1 \le N-1 \\ c_{j-2i+1+n} & \text{when } j-2i+1 < 0 \\ 0 & \text{when } j-2i+1 \ge N \end{cases} \quad (8)$$

Step 6. Similarly, let us define H_n filter for $\mathrm{I}[m,n,k]$, filter for $H_n[i,j]$ element i, j of H_n, and define it as:

$$H_n[i,j] = \begin{cases} (-1)^{j+1} c_{j-2i+1} & \text{when } 0 \le 2i-j \le N-1 \\ (-1)^{j+1} c_{2i-j+n} & \text{when } 2i-j < 0 \\ 0 & \text{when } 2i+1 \ge N \end{cases} \quad (9)$$

$L_n[i,j]$ and $H_n[i,j]$ are defined for i=1,2,...$n/2$ and j=1,2,...n, so that L_n and H_n are the matrices with $n/2 \times n$ size.

The result will be included in the matrix $\mathrm{I}_{Db}^{\Psi}[m,n,k]$

Transformations of L and H Daubechies filters for hyperspectral AI are presented in the matrix D_w:

Scientific Journal of Astana IT University
ISSN (P): 2707-9031 ISSN (E): 2707-904X
VOLUME 15, SEPTEMBER 2023

$$\begin{pmatrix} c_1 & c_2 & c_3 & c_4 & 0 & 0 & 0 & 0 \\ c_4 & -c_3 & c_2 & -c_1 & 0 & 0 & 0 & 0 \\ 0 & 0 & c_1 & c_2 & c_3 & c_4 & 0 & 0 \\ 0 & 0 & c_4 & -c_3 & c_2 & -c_1 & 0 & 0 \\ 0 & 0 & 0 & 0 & c_1 & c_2 & c_3 & c_4 \\ 0 & 0 & 0 & 0 & c_4 & -c_3 & c_2 & -c_1 \\ 0 & 0 & 0 & 0 & 0 & 0 & c_1 & c_2 \\ 0 & 0 & 0 & 0 & 0 & 0 & c_4 & -c_3 \end{pmatrix} * \begin{bmatrix} 123 \\ 105 \\ 121 \\ 103 \\ 118 \\ 100 \\ 123 \\ 123 \end{bmatrix} = \begin{bmatrix} L \\ H \\ L \\ H \\ L \\ H \\ L \\ H \end{bmatrix}, \quad (10)$$

where $D_w \bullet \mathrm{I}[m,n,k] = D_w^{'}[C,K]$.

After coding, the wavelet coefficients of the low-frequency and high-frequency components are obtained, L and H, respectively, which are subsequently subject to quantization.

When restoring the original image channels, as in the previous example of the Haar wavelet, the resulting matrix is subject to transposition. An example of the inverse Daubechies transform:

$$\begin{pmatrix} c_1 & c_4 & 0 & 0 & 0 & 0 & 0 & 0 \\ c_2 & -c_3 & 0 & 0 & 0 & 0 & 0 & 0 \\ c_3 & c_2 & c_1 & c_4 & 0 & 0 & 0 & 0 \\ c_4 & -c_1 & c_2 & -c_3 & 0 & 0 & 0 & 0 \\ 0 & 0 & c_3 & c_2 & c_1 & c_4 & 0 & 0 \\ 0 & 0 & c_4 & -c_1 & c_2 & -c_3 & 0 & 0 \\ 0 & 0 & 0 & 0 & c_3 & c_2 & c_1 & c_4 \\ 0 & 0 & 0 & 0 & c_4 & -c_1 & c_2 & -c_3 \end{pmatrix} * \begin{bmatrix} L \\ H \\ L \\ H \\ L \\ H \\ L \\ H \end{bmatrix} = \begin{bmatrix} 123 \\ 105 \\ 121 \\ 103 \\ 118 \\ 100 \\ 123 \\ 123 \end{bmatrix}, \quad (11)$$

where $D_w^T \bullet D_w^{'}[C,K] = \mathrm{I}[m,n,k]$.

The difference between the Daubechies wavelet transform and the Haar wavelet is that the identification of low-frequency areas of the image is performed by changing the filter operators. This gives good quality at a low compression ratio and is inferior to the Haar wavelet.

Now, let's examine the orthogonal Walsh-Hadamard transform that follows.

Walsh-Hadamard transform.

For a given fragment of hyperspectral AI channels I_{mn}, its two-dimensional forward and inverse Walsh-Hadamard transform (WHT) are determined using the following formulae (12) and (4):

$$\mathrm{H}(u,\upsilon) = \frac{1}{L}\sum_{M=0}^{L-1}\sum_{N=0}^{L-1} \mathrm{I}_{mn} g(-1)^{\sum_{i=0}^{J}[b_i(m)p_i(u)+b_i(n)p_i(v)]} \quad (12)$$

$$\mathrm{I}_{mn} = \sum_{u=0}^{L-1}\sum_{v=0}^{L-1} H(u,v)h(m,n,u,v) = \frac{1}{L}\sum_{m=0}^{L-1}\sum_{n=0}^{L-1} H(u,v)(-1)^{\sum_{i=0}^{J}[b_i(m)p_i(u)+b_i(m)p_i(v)]}, \quad (13)$$

where $H(u, v)$ – is the result from transformation (i.e. *WHT coefficients*), the value of $b(u)$ is equal to bit i in binary integer representation u, and $p_i(u)$ is defined as $b_j(u)$ from the following recurrence relations (14):

DOI: 10.37943/15DLPO1951

$$
\begin{aligned}
p_o(u) &= b_{n-1}(u),\\
p_1(u) &= b_{n-1}(u) + b_{n-2}(u),\\
p_2(u) &= b_{n-2}(u) + b_{n-3}(u),\\
p_{n-1}(u) &= b_1(u) + b_0(u),
\end{aligned}
\tag{14}
$$

The quantities $g(x, y, u, v)$ and $h(x, y, u, v)$ are called kernels (or basis images) *WHT*, and their matrices are the same. The elements of matrices are numbers +1 and -1, which are multiplied by $1/N$. In the result of transformation, the *WHT* consists of multiplication of pixels by *+1* or *-1*, addition and division of the sum by N.

Let's take an example to illustrate the transformation of a segment of hyperspectral AI. Let the fragment of the AI is defined in the form of the matrix, which consists of m rows, n columns and k channels: $\mathrm{I}[m, n, \mathrm{k}] = \mathrm{I}[10, 10, 10]$.

WHT transformations can be viewed as filters that partition an image into its low-frequency and high-frequency components. In order to reconstruct the original image, it is simply a matter of recombining these components.

Direct WHT transform is defined in the matrix form H_{wt2}, the fragment of AI has been taken, which means $H_{wt2} \bullet \mathrm{I}[m,n,k] = H_{wt2}'[CK]$, where CK – spectral component of the matrix $\mathrm{I}[m, n, k]$.

$$
\begin{pmatrix}
\frac{1}{2} & \frac{1}{2} & 0 & 0 & 0 & 0 & 0 & 0 & 0 & 0\\
\frac{1}{2} & -\frac{1}{2} & 0 & 0 & 0 & 0 & 0 & 0 & 0 & 0\\
0 & 0 & \frac{1}{2} & \frac{1}{2} & 0 & 0 & 0 & 0 & 0 & 0\\
0 & 0 & \frac{1}{2} & -\frac{1}{2} & 0 & 0 & 0 & 0 & 0 & 0\\
0 & 0 & 0 & 0 & \frac{1}{2} & \frac{1}{2} & 0 & 0 & 0 & 0\\
0 & 0 & 0 & 0 & \frac{1}{2} & -\frac{1}{2} & 0 & 0 & 0 & 0\\
0 & 0 & 0 & 0 & 0 & 0 & \frac{1}{2} & \frac{1}{2} & 0 & 0\\
0 & 0 & 0 & 0 & 0 & 0 & \frac{1}{2} & -\frac{1}{2} & 0 & 0\\
0 & 0 & 0 & 0 & 0 & 0 & 0 & 0 & \frac{1}{2} & \frac{1}{2}\\
0 & 0 & 0 & 0 & 0 & 0 & 0 & 0 & \frac{1}{2} & -\frac{1}{2}
\end{pmatrix}
*
\begin{bmatrix} 123\\105\\121\\103\\118\\100\\123\\123\\122\\104 \end{bmatrix}
=
\begin{bmatrix}
\frac{123}{2}+\frac{105}{2}\\
\frac{123}{2}-\frac{105}{2}\\
\frac{121}{2}+\frac{103}{2}\\
\frac{121}{2}-\frac{103}{2}\\
\frac{118}{2}+\frac{100}{2}\\
\frac{118}{2}-\frac{100}{2}\\
\frac{123}{2}+\frac{123}{2}\\
\frac{123}{2}-\frac{123}{2}\\
\frac{122}{2}+\frac{104}{2}\\
\frac{122}{2}-\frac{104}{2}
\end{bmatrix}
=
\begin{bmatrix}
\frac{228}{2}\\
\frac{18}{2}\\
\frac{224}{2}\\
\frac{18}{2}\\
\frac{218}{2}\\
\frac{18}{2}\\
\frac{246}{2}\\
0\\
\frac{226}{2}\\
\frac{18}{2}
\end{bmatrix}
\tag{15}
$$

After performing this transformation, we acquire coefficients for both the low-frequency and high-frequency components, precisely as follows: $\mathrm{CK} = 114, 9, 112, 9, 114, 9, 123, 0, 123, 9$. In the quantization phase, high-frequency coefficients that are in proximity to zero or in the negative range are rounded down to zero. It's important to mention that the computation of matrices for levels H_{wt4} and H_{wt8} follows the same procedure as for H_{wt2}.

At the stage of reconstruction of the original image channels, the "CK" decoding occurs. The example of the inverse transform is provided as follows:

Scientific Journal of Astana IT University
ISSN (P): 2707-9031 ISSN (E): 2707-904X
VOLUME 15, SEPTEMBER 2023

$$\begin{pmatrix} \frac{1}{2} & \frac{1}{2} & 0 & 0 & 0 & 0 & 0 & 0 & 0 & 0 \\ \frac{1}{2} & -\frac{1}{2} & 0 & 0 & 0 & 0 & 0 & 0 & 0 & 0 \\ 0 & 0 & \frac{1}{2} & \frac{1}{2} & 0 & 0 & 0 & 0 & 0 & 0 \\ 0 & 0 & \frac{1}{2} & -\frac{1}{2} & 0 & 0 & 0 & 0 & 0 & 0 \\ 0 & 0 & 0 & 0 & \frac{1}{2} & \frac{1}{2} & 0 & 0 & 0 & 0 \\ 0 & 0 & 0 & 0 & \frac{1}{2} & -\frac{1}{2} & 0 & 0 & 0 & 0 \\ 0 & 0 & 0 & 0 & 0 & 0 & \frac{1}{2} & \frac{1}{2} & 0 & 0 \\ 0 & 0 & 0 & 0 & 0 & 0 & \frac{1}{2} & -\frac{1}{2} & 0 & 0 \\ 0 & 0 & 0 & 0 & 0 & 0 & 0 & 0 & \frac{1}{2} & \frac{1}{2} \\ 0 & 0 & 0 & 0 & 0 & 0 & 0 & 0 & \frac{1}{2} & -\frac{1}{2} \end{pmatrix} * \begin{bmatrix} \frac{228}{2} \\ -\frac{18}{2} \\ \frac{224}{2} \\ \frac{18}{2} \\ \frac{218}{2} \\ \frac{18}{2} \\ \frac{246}{2} \\ 0 \\ \frac{226}{2} \\ \frac{18}{2} \end{bmatrix} \begin{bmatrix} \frac{228}{2}+\frac{18}{2} \\ \frac{228}{2}-\frac{18}{2} \\ \frac{224}{2}+\frac{18}{2} \\ \frac{224}{2}-\frac{18}{2} \\ \frac{218}{2}+\frac{18}{2} \\ \frac{218}{2}-\frac{18}{2} \\ \frac{246}{2}+0 \\ 0 \\ \frac{226}{2}+\frac{18}{2} \\ \frac{226}{2}-\frac{18}{2} \end{bmatrix} = \begin{pmatrix} \frac{246}{2} \\ \frac{210}{2} \\ \frac{242}{2} \\ \frac{206}{2} \\ \frac{236}{2} \\ \frac{200}{2} \\ \frac{246}{2} \\ 0 \\ \frac{246}{2} \\ \frac{208}{2} \end{pmatrix} \quad (16)$$

Here $H_{wt2}^{T} \cdot H_{wt2}'[CK] = \mathrm{I}[m,n,k]$, where H_{wt2}^{T} – inverse *WHT* transform, $H_{wt2}'[CK]$ – spectral component.

By modify the basis of the matrix (H_4, H_8) for each submatrix, conducting both forward and inverse computations. During this process, we calculate each element of the transformed submatrix using the following formulas:

$$WHT = \frac{\sum_{i=1}^{n} I[m,n,k] \times H_w[i,j]}{2^H} \quad (17)$$

$$WHT_D = \sum_{i=1}^{n} \mathrm{I}[m,n,k] \times H_w[i,j] \times H \quad (18)$$

where n – size of the Hadamard matrix, $\mathrm{I}[m,n,\mathrm{k}]$ – submatrix of the original matrix, H_w – Hadamard matrix, i – row of current value in submatrix, j – current value column in submatrix, H – basis of the matrix.

One of the benefits of employing the Walsh-Hadamard transform is its enhanced capability to identify low-frequency components. This is achieved by segmenting hyperspectral AI channel regions into sublayers. This gives average compression rates with average image quality.

Results

Dataset. Hyperspectral aerospace images available in the public domain are used as test data. The compression results are compared with universal archivers and algorithms.

In order to assess the performance of the suggested algorithm in terms of compression ratio and to identify its practical boundaries, a series of experiments were carried out using Hyperspectral Anomaly Index (HAI) data from the AVIRIS remote sensing system. These experiments utilized the data in the format compatible with the Idrisi Kilimanjaro raster geoinformation system. AVIRIS (Airborne Visible / Infrared Imaging Spectrometer) system – provides

DOI: 10.37943/15DLPO1951

simultaneous reception of 220 spectral images with wavelengths ranging from 400 nm and 2500 nm.

The experimentation took place on a computer equipped with an Intel Core i7 processor, which operates at a clock speed of 2.5 GHz, and boasts a memory capacity of 16 GB. The computer was running the Windows 10 operating system, as detailed in Table 1.

Table 1. Examples of test data characteristics (AVIRIS remote sensing systems) by scene size

Name of hyperspectral AI	K, number of channels	M N, pixels	File size, bytes
a196715p11k_23_r07_ pt11	220	120 120	62056005
a196715p11k_23_r07_ pt12	220	220 220	37032219
a196715p11k_23_r07_ pt13	220	320 320	95416506
a196715p11k_23_r07_ pt14	220	420 420	105102549
a196715p11k_23_r07_pt15	220	520 520	225453345
a196715p11k_23_r07_pt16	220	620 512	286546543

Experimental results for the proposed hyperspectral image preprocessing algorithm considering data specificity and inter-channel correlation.

Let's consider the results of preparatory processing experiments based on wavelet and orthogonal transformations before compressing hyperspectral AI with minimizing the loss level.

The following possible stages of preparatory processing of hyperspectral AI based on the proposed stages: The data structure was modified by encoding wavelet coefficients derived from the original hyperspectral Anomaly Index (AI) data. This transformation was exemplified through the utilization of one-dimensional and two-dimensional Haar wavelets, Daubechies coefficients, and the Walsh-Hadamard transform. To evaluate the efficiency of the proposed algorithm in relation to compression ratios and to ascertain its practical constraints, several experiments were conducted using hyperspectral AI data.

The compression ratios of the Haar, Daubechies and Walsh-Hadamard wavelet transforms are shown in Fig. 1.

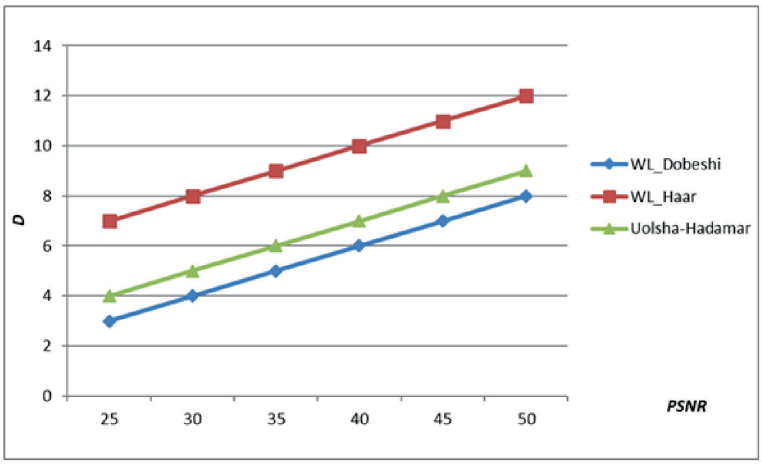

Figure 1. Compression ratio D and PSNR loss rates

As can be seen from Fig. 1, the compression ratios of the one-dimensional and two-dimensional Haar wavelet lossy transforms are superior in compression ratio to the Daubechies

Scientific Journal of Astana IT University
ISSN (P): 2707-9031 ISSN (E): 2707-904X
VOLUME 15, SEPTEMBER 2023

wavelet of the JPEG Lossy compressor. The suggested lossy approach is delineated by adaptive transformations that rely on both the Haar and Daubechies wavelet transforms. This approach involves the application of a predetermined quantization step followed by subsequent arithmetic coding with a specific rate $(R = 16)$. The results garnered from the comparative analysis of the transformed HAI employing the derived wavelet coefficients strongly indicate the efficacy of the preparatory procedures.

Examples of one-dimensional and two-dimensional Haar wavelet transforms, Fig. 2 (a, b), $K = 2, 3, 10$.

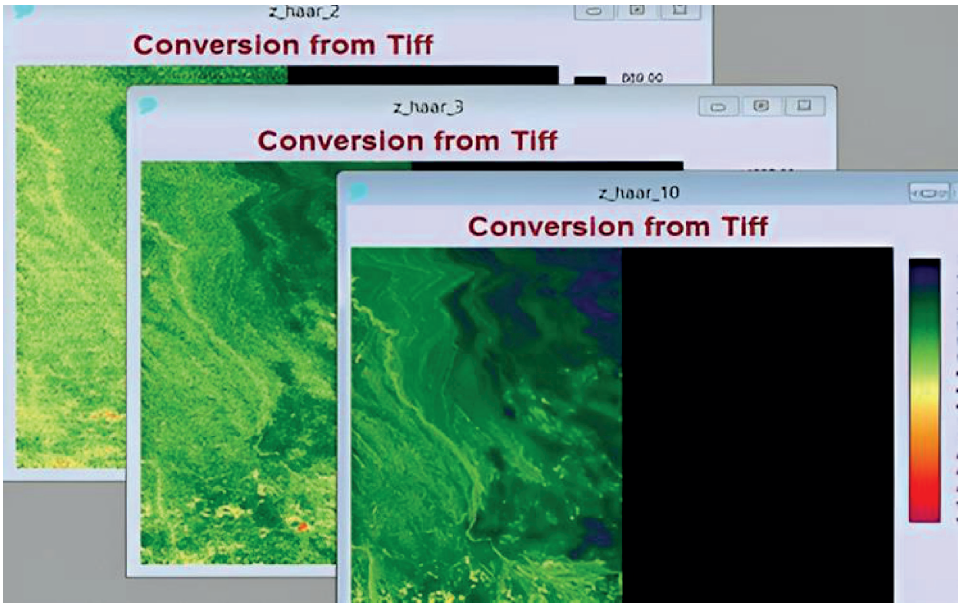

(a) one-dimensional

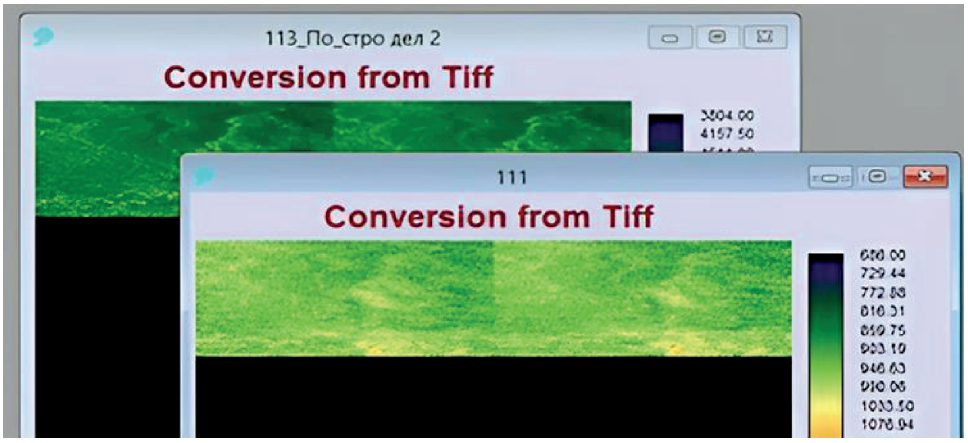

b) two-dimensional

Figure 2. Haar wavelet transform

Examples of the Daubechies wavelet transform, Fig. 3, $K = 1, 4$.

DOI: 10.37943/15DLPO1951

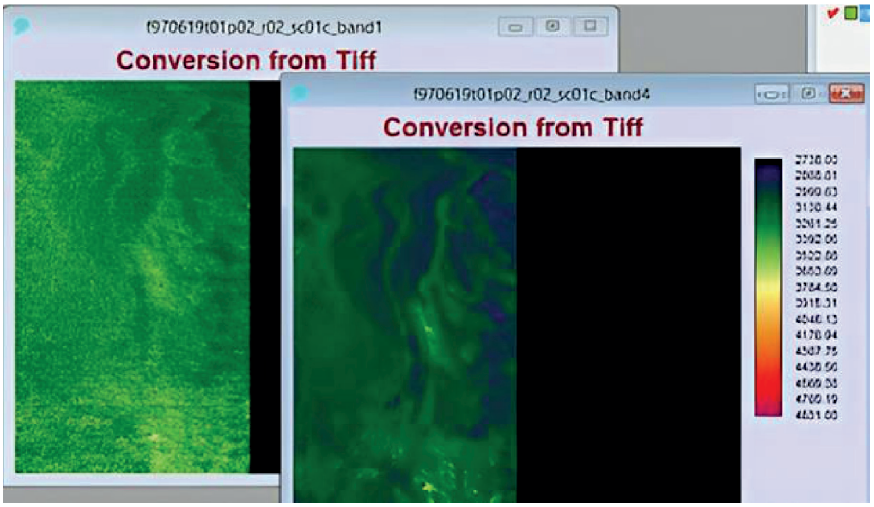

Figure 3. Daubechies wavelet transform

Examples of reconstructed Walsh-Adamar HAI transforms (1,2,3 levels), $K = 10$, are presented on Fig. 4.

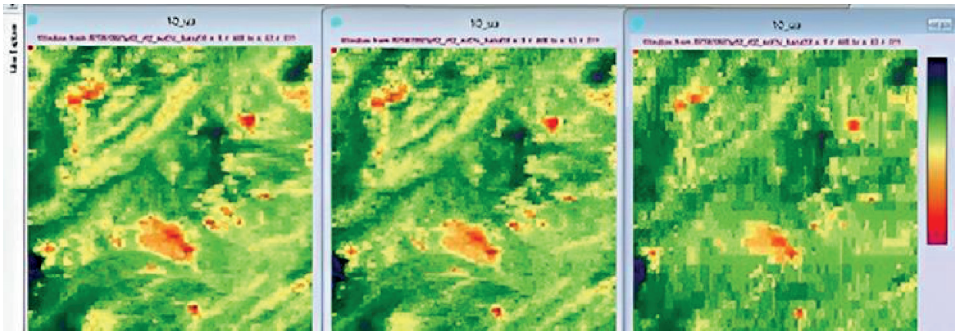

Figure 4. Reconstructed images after Walsh-Adamar

Original image, $K = 10$, is presented on Fig. 5.

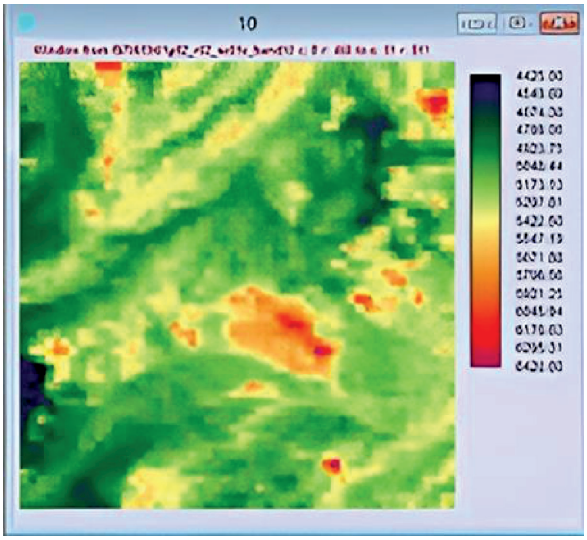

Figure 5. The original image

Scientific Journal of Astana IT University
ISSN (P): 2707-9031 ISSN (E): 2707-904X
VOLUME 15, SEPTEMBER 2023

The quality assessment of the recovered images was established through the utilization of PSNR and SKO. The extent of distortion measures the balance between compression and degradation in lossy algorithms. This score is characterized as the mean number of bits required to depict each individual pixel.

Conclusion

As a result of the research conducted in the pursuit of developing an algorithm for the preprocessing of Hyperspectral Aerospace Images (HAI) before compression, a series of experiments were conducted. These experiments involved the transformation of the data structure based on the original HAI with a focus on the storage of wavelet coefficients. Specifically, the Haar wavelet was employed as an illustrative example. Additionally, transformations of the data structure derived from the original hyperspectral Aerospace Image, storing wavelet coefficients using the Daubechies wavelet, including both low-frequency and high-frequency coefficients, were examined. Furthermore, transformations of the data structure originating from the original HAI, concentrating on coefficient values, were investigated with the utilization of the discrete-cosine transformation. A three-level Walsh-Hadamard transformation was also applied in the experimental process. The experimental indicators are significantly superior to some previous algorithms of individual developments in terms of the compression ratio, peak signal-to-noise ratio, as well as the variability of the data used in terms of the size of HAI and considering the specifics of the data.

Based on the above results of the experiment on preprocessing based on orthogonal and wavelet transforms of hyperspectral lossy aerospace images, it can be concluded that the developed mathematical and software compression, to some extent, leads in terms of compression ratio and quality of reconstructed images depending on the selected preprocessing. The developed HAI preprocessing algorithm and compression significantly reduce the original data's size while preserving the necessary information. This opens opportunities for more efficient transmission and storage of hyperspectral images, reducing the load on storage and network channels. Despite the data compression, the quality of the recovered images remains high. This means that important details and data structures are preserved, critical for accurate analysis and interpretation of hyperspectral data. The developed algorithm not only matches but also outperforms existing analogues. This indicates its competitiveness and significant potential for application in real-world problems. An important aspect is the algorithm's flexibility which allows for choosing the best preprocessing method depending on the characteristics and requirements of specific data. The algorithm can be successfully applied to various hyperspectral image sets.

The results obtained are essential for hyperspectral data processing and can find applications in various fields such as aerospace technology, geomorphology, and agriculture. Using the prospect of continuing long-term research in the field of hyperspectral image processing, data-specific learning algorithms using neural network methods are being developed to expand the package of original images from various remote sensing spacecraft, which will provide more comprehensive and generalized results in the field of hyperspectral image processing.

Acknowledgement

Authors express sincere gratitude to Astana IT University for the invaluable support and resources throughout the duration of this research project.

Funding

The article was written within the state order for the implementation of the scientific program under the budget program of the Republic of Kazakhstan 217 "Development of Science", subprogram 101 "Program-targeted funding of the scientific and/or technical activity at the expense of the national budget" on the theme: "Development of technology for intelligent preprocessing of aerospace images for recognition and identification of various objects " Grant IRN AP19678773.

References

[1] Wang, Z., Xiao, H., He, M., Wang, L., Xu, K., & Nian, Y. (2020). Spatial-Spectral Joint Compressed Sensing for Hyperspectral Images. *IEEE Access*, 8, 149661-149675. https://doi.org/10.1109/ACCESS.2020.3014350

[2] Llaveria, D., Camps, A., Park, H., & Narayan, R. (2022). Ranking Methodology for Sequential Band Selection Combining Data Dispersion and Spectral Band Correlation. *IEEE International Geoscience and Remote Sensing Symposium*, 775-778. https://doi.org/10.1109/IGARSS46834.2022.9884380

[3] Mijares i Verdú, S., Ballé, J., Laparra, V., Rapesta, J.B., Hernández-Cabronero, & Serra-Sagristá, M.J. (2022). Hyperspectral remote sensing data compression with neural networks. *UT, USA: Data Compression Conference (DCC)*, 476-476. https://doi.org/10.1109/DCC52660.2022.00087.

[4] Chen, Y. & Yuan, F. (2021). Research on Lossless Compression of Hyperspectral Images Based on Improved Deep Learning Algorithm. *Chongqing, China: International Conference on Intelligent Computing, Automation and Systems (ICICAS),* 111-116. https://doi.org/10.1109/ICICAS53977.2021.00029

[5] Pestel-Schiller, U., Hu, K., Gritzner, D., & Ostermann, J. (2021). Determination of Relevant Hyperspectral Bands Using a Spectrally constrained CNN. *Amsterdam, Netherlands: 11th Workshop on Hyperspectral Imaging and Signal Processing: Evolution in Remote Sensing (WHISPERS),* 1-5. https://doi.org/10.1109/WHISPERS52202.2021.9483986

[6] Gandikota, D.M., Gladkova, T., Tran, K.A., Bapat, S., Richkus, J., & Arnold, D.J. (2022). AI Augmentation to Remote Sensing Imagery in Forestry Conservation & Restoration for Increased Responsive Capabilities. *IEEE Applied Imagery Pattern Recognition Workshop (AIPR),* 1-16. https://doi.org/10.1109/AIPR57179.2022.10092215

[7] Ali, B.H.B.F., Prakash, R. (2021) Overview on Machine Learning in Image Compression Techniques *IEEE International Virtual Conference on Innovations in Power and Advanced Computing Technologies, i-PACT 2021*, 3rd https://doi.org/10.1109/i-PACT52855.2021.9696987

[8] Sucharitha, B., & Anitha Sheela, K. (2022). Hyper Spectral Image compression using Higher Order Orthogonal Iteration Tucker decomposition. *Kochi, India: 2022 IEEE 19th India Council International Conference (INDICON)*, 1-7. https://doi.org/10.1109/INDICON56171.2022.10040093

[9] Kapah, L., Weizman, N., Bykhovsky, D., & August, I.Y. (2022). Hyper-Spectral Image Compression By Joint Spatial Spectral Dimension Reduction Using Thresholded Principal Component Analysis. *Rome, Italy: 2022 12th Workshop on Hyperspectral Imaging and Signal Processing: Evolution in Remote Sensing (WHISPERS)*, 1-5. https://doi.org/10.1109/WHISPERS56178.2022.9955095

[10] Chandra, H., & Bajpai, S. (2022). Listless Block Cube Tree Coding for Low Resource Hyperspectral Image Compression Sensors. *Aligarh, India: 2022 5th International Conference on Multimedia, Signal Processing and Communication Technologies (IMPACT),* 1-5. https://doi.org/10.1109/IMPACT55510.2022.10029076

[11] Ahanonu, E., Marcellin, M.W., & Bilgin, A. (2019). Clustering Regression Wavelet Analysis for Lossless Compression of Hyperspectral Imagery. *Snowbird, UT, USA: 2019 Data Compression Conference (DCC),* 551-551. https://doi.org/10.1109/DCC.2019.00063

[12] Mei, S., Khan, B. M., Zhang, Y., & Du, Q. (2018). Low-Complexity Hyperspectral Image Compression Using Folded PCA and JPEG2000. *Valencia, Spain: IGARSS 2018 - 2018 IEEE International Geoscience and Remote Sensing Symposium,* 4756-4759. https://doi.org/10.1109/IGARSS.2018.8519455

Scientific Journal of Astana IT University
ISSN (P): 2707-9031 ISSN (E): 2707-904X
VOLUME 15, SEPTEMBER 2023

[13] Wang, Z. (2021). Entropy Analysis for Clustering Based Lossless Compression of Remotely Sensed Image. *Orlando, FL, USA: 2021 IEEE International Conference on Big Data (Big Data)*, 4220-4223. https://doi.org/10.1109/BigData52589.2021.9671694

[14] Chandra, H., & Bajpai, S. (2023). 3D-Block Partitioning Embedded Coding for Hyperspectral Image Sensors. *Aligarh, India: 2023 International Conference on Power, Instrumentation, Energy and Control (PIECON)*, 1-5. https://doi.org/10.1109/PIECON56912.2023.10085841

[15] Sarinova, A.J., & Isin, M.E. (2016). Coding and decoding of hyperspectral aerospace images using wavelet transforms. Modern knowledge-intensive technologies. Regional application. №4 (48). cyberleninka.ru/article/n/kodirovanie-i-dekodirovanie-giperspektralnyh-aerokosmicheskih-izo-brazheniy-s-primeneniem-veyvlet-preobrazovaniy

[16] Dunayev, P., Bekbayeva, A., Mekhtiyev, A., & Sarsikeyev, Y. (2022). Development of compression algorithms for hyperspectral aerospace images based on discrete orthogonal transformations. Eastern-European Journal of Enterprise Technologiesthis link is disabled, 1(2-115), 22 – 30. http://journals.uran.ua/eejet/article/view/251404/250664

[17] Sarinova, A. (2021). Development of compression algorithms for hyperspectral aerospace images based on discrete orthogonal transformations. *E3S Web of Conferences*, 333, 01011. http://dx.doi.org/10.1051/e3sconf/202133301011

[18] Sarinova, A. & Zamyatin, A. (2020) Hyperspectral regression lossless compression algorithm of aerospace images. *E3S Web of Conferences*, 149, 02003. https://doi.org/10.1051/e3sconf/202014902003

[19] Sarinova, A., Lisnevskyi, R., Biloshchytskyi, A., & Akizhanova, A. (2022). The Lossless Compression Algorithm of Hyperspectral Aerospace Images with Correlation and Bands Grouping. *Nur-Sultan: SIST 2022 - 2022 International Conference on Smart Information Systems and Technologies, Proceedings*. https://doi.org/10.1109/SIST54437.2022.9945821

[20] Sarinova, A., Neftissov, A., & Bronin, S. (2022). Regression Approach to Lossles Compression Algorithm for Hyperspectral Images. *Nur-Sultan: SIST 2022 - 2022 International Conference on Smart Information Systems and Technologies, Proceedings*. https://doi.org/10.1109/SIST54437.2022.9945817